# Onset of plasticity of helium irradiation ferritic/martensitic steels during nanoindentation

S. Chen*, Y. Wang, N. Hashimoto, S. Ohnuki

*Graduate School of Engineering, Hokkaido University, N-13, W-8, Sapporo 060-8278, Japan*

## Abstract

Nanoindentation techniques have been developed to determine the hardness of ion-irradiated materials. However, the incipient plasticity during nanoindentation is a new method to investigate the irradiation damage of structural materials in fusion reactor. In this paper, helium implanted F82H-IEA and nano-sized oxide dispersion strengthened F82H-ODS steels were used to study the elastic-plastic transition at a constant loading rate. The onset of plasticity shifted after helium implantation. By a statistical thermal activation model we extract activation volume of F82H-IEA and F82H-ODS with and without He, respectively. The results reveal an increasing pinning force and number density of effective obstacles over dislocations in He-implanted

* Corresponding author. Tel.: +81 11 706 6772.

*E-mail address*: chensiwei@eng.hokudai.ac.jp (S. Chen).

F82H-IEA, but a weakening local pinning force without changing the density of effective obstacles in He-implanted F82H-ODS.

Keywords: incipient plasticity, helium irradiation, oxide particle, nanoindentation

## 1. Introduction

Nanoindentation techniques have been developed to measure the hardness of ion-irradiated specimens using load and displacement sensing indentation experiment[1-7]. Loads with nanonewton-level and displacements with angstrom-level can be accurately measured[8, 9]. A further issue in load-penetration depth curves, onset of plasticity, has been studied to understand the mechanisms governing defect nucleation. The onset of plasticity usually indicates by a first burst of displacement, as the indenter tip ‘pops’ into the specimen[10-16]. The typical indentation depth of onset of plasticity is below tens of nm. The simulations of the initial defect nucleation event in single <111> Cu have shown that the nucleation site of defect is at a depth ~60% of the contact radius[17], far below the surface. Recent studies put a quantitative insight into the incipient plasticity and present a statistical thermal activation model to determine the

activation energy and volume for the onset of plasticity during nanoindentation[9, 18]. However, this model has not been used to understand the mechanical property evolution in irradiation damage field.

F82H-IEA and F82H-ODS steels are candidates for structural materials in fusion reactor. The degradation of mechanical property of structural materials caused by transmuted helium in fusion reactor is one of outstanding issues.

In this paper, helium ions were injected into samples to discuss the onset of plasticity of F82H-IEA and F82H-ODS steels with and without He, respectively, and extract the activation volume from experiment data. The roles of nano-sized oxide particles and implanted helium in the onset of plasticity are also studied.

## 2. Experimental procedures and methodology

Two steels, F82H-IEA and F82H-ODS (both provided by the Japan Atom Energy Agency), were fabricated into 3mm diameter disks with a thickness of 0.15mm. The chemical compositions and heat treatment conditions of the specimens of the two steels are shown in Table 1[19, 20]. All the samples were electro-polished to remove the deformation zone and obtain a smooth surface. Helium ions at 70 - 250 keV were injected into the samples at room temperature. Fig. 1 shows the Stopping and Range of

Ions in Matter (SRIM) calculations of the profile of the implanted helium and the displacement damage. The helium concentration was at an approximately constant 0.2 at. %. The implanted region is 800 nm from the surface.

Nano-indentation was performed using an Elionix ENT-1100a (Elionix Inc. Japan) nano-indenter with Berkovich-type tip. Indentations were placed 5 um apart from one another and the typical indentation depth was below 30 nm with a maximum load of 40-120 μN. Between indentations, the tip was maintained in contact with the specimen surface at a very low set-point load of 2μN, which prevents issues of jump to contact prior to indentation, as well as artifacts related to indenter momentum during approach[9, 21]. The temperature of the system during nanoindentation was 28 ºC, and the loading rate is 6μN $s^{-1}$. Fig. 2 shows a typical load-displacement (P-h) curve for nanoindentation with first displacement burst marked with black arrow. 250 P-h curves were obtained from indentations for each sample.

The statistical thermal activation model is provided by J. K. Mason et al[9, 18]. By a series of nominally identical indentations, the statistical distributions for the first displacement burst can be derived, and the ultimate function between the load (P) and cumulative fraction function (F) for the statistics of the first burst is expressed as the function:

$$\ln\left[\ln\left(\frac{1}{1-F(P)}\right)\right]=\alpha P^{1/3}+\beta. \qquad (1)$$

Here the parameter α and β are constants from experimental data. The activation volume is extracted from the measured slope of curves α, and is given by

$$V=\frac{\pi}{0.47}\left(\frac{3\rho}{4E_R}\right)^{2/3} kT\cdot\alpha, \qquad (2)$$

where ρ is the radius of the indenter tip and $E_R$ is the reduced modulus of the tip-sample combination.

**3. Results and discussion**

Fig. 3 shows the statistical data acquired for the first displacement burst during nanoindentation. The loads, P, at the first burst point are identified from p-h curves, and then the cumulative fraction of loads at the first burst point is plotted in Fig. 3. In the 250 indentations of F82H-IEA, 60% of the loads at the first burst point are below 20 μN. In the meantime, the load for F82H-ODS at the same cumulative fraction is 60μN. The results suggest that the hardness of F82H-ODS is higher than F82H-IEA. After helium implantation, the F-P curve of F82H-IEA shifted to the load increasing direction, and the curve of F82H-ODS shifted to the load decreasing direction, as shown by the black arrows. The results suggest that He implantation causes an enhanced local pinning force

over dislocations in F82H-IEA, but a weakening pinning force over dislocations in F82H-ODS.

Fig. 4 shows the linear form transformed from the cumulative distribution function to extract the activation volume. The slope of the line for F82H-IEA is apparently changed after He implantation, whereas there is no change of linear slope for F82H-ODS. Further, the slope of the line which presents helium implanted F82H-IEA is close to the slope of the lines presenting F82H-ODS and He implanted F82H-ODS. In the previous study, we have observed cavities in the matrix of F82H-IEA and F82H-ODS, formed by He implantation. The similar slope reveals that cavities and oxide particles have a similar response to activation volume. Table 2 presents activation volumes which are extracted from Fig. 4 [22]. The activation volume is defined as the total volume of coherently activated atoms, multiplied by their transformation strain[23]. The activation volume of He implanted F82H-IEA is rather smaller than F82H-IEA, indicating an increasing density of effective obstacles to dislocations. The activation volume of He implanted F82H-ODS is the same with F82H-ODS, revealing that the density of effective obstacles have no significant change.

## 4. Conclusions

Incipient plasticity analysis during nanoindentation was applied to helium irradiation ferritic/martensitic steels. Activation volume of F82H-IEA and F82H-ODS with and without He, respectively, is figured out from experiment data. Helium implantation causes an enhanced local pinning force and an increasing density of effective obstacles over dislocations in F82H-IEA, but a weakening local pinning force without changing the density of effective obstacles in F82H-ODS. The incipient plasticity during nanoindentation is useful to investigate the irradiation damage of structural materials in fusion reactor.

**Reference**


1. W. C. Oliver, G. M. Pharr, J. Mater. Res. **7,** 1564 (1992).
2. S. J. Zinkle, W. C. Oliver, J. Nucl. Mater. **141-143,** 548 (1986).
3. H. Ullmaier, E. Camus, J. Nucl. Mater. **251**, 262 (1997).
4. R. Kasada Y. Takayama, K. Yabuuchi, A. Kimura, Fusion Eng. and Des. **86,** 2658 (2011).
5. P. M. Rice, R. E. Stoller, MRS proceedings. 649 (2000).
6. N. Li, M. Nastasi, A. Misra, International Journal of Plasticity. **32-33**, 1 (2012).
7. C. Robertson, B. K. Panigrahi, S. Balaji, S. Kataria, Y. Serruys, M. H. Mathon, C. S. Sundar, J. Nucl. Mater. **426**, 240 (2012).
8. X. Li, B. Bhushan, Materials Characterization. **48**, 11 (2002).
9. J. K. Mason, A. C. Lund, C. A. Schuh, Phys. Rev. B **73**, 054102 (2006).

10. W. W. Gerberich, S. K. Venkataraman, H. Huang, S. E. Harvey, D. L. Kohlstedt, Acta Metall. mater. **43**, 1569 (1995).

11. W. W. Gerberich, J. C. Nelson, E. T. Lilleodden, P. Anderson, J. T. Wyrobek, Acta Mater. **44**, 3585 (1996)

12. S. Suresh, T. -G. Nieh, B. W. Choi, Scripta Mater. 41, 951 (1999).

13. J. D. Kiely, J. E. Houston, Phys. Rev. B **57**, 12588 (1998).

14. T. A. Michalske, J. E. Houston, Acta Mater. **46**, 391 (1998).

15. A. Gouldstone, H. -J. Koh, K. -Y. Zeng, A. E. Giannakopoulos, S. Suresh, Acta Mater. **48**, 2277 (2000).

16. T. F. Page, W. C. Oliver, C. J. McHargue, J. Mater. Res. **7**, 450 (1992).

17. J. Li, K. J.Van Vliet, T. Zhu, S. Yip, S. Suresh, nature **418**, 307 (2002).

18. C. A. Schuh, J. K. Mason, A. C. Lund, Nat. Mater. **4**, 617 (2005).

19. H. Tanigawa, A. Sawahata, M. A. Sokolov, M. Enomoto, R. L. Klueh, A. Kohyama, Mater. Trans. **48**, 570 (2007) .

20. K. Shinozuka, H. Esaka, M. Tamura and H. Tanigawa: J. Nucl. Mater. **417**, 233 (2011) .

21. A. B. Mann, J. B. Pethica, Philos. Mag. A **79**, 577 (1999).

22. K. Shiba, N. Yamanouchi, A. Tohyama, Fusion Materials Semi-Annual Progress Reports **20**, 190 (1996).

23. A. G. Khachaturyan, Theory of Structural Transformation in Solids (Wiley, New York, 1983)

Figure captions

Fig.1. SRIM calculations for the He implantation, with the concentration 0.2 at.% and displacement damage 0.1 dpa.

Fig. 2. A typical load-displacement (P-h) curve for nanoindentation. The arrow indicates the first displacement burst.

Fig. 3. The plot of the cumulative fraction, F, and applied loads, P, at the burst point.

Fig. 4. Linear relation used to extract the activation volume. The solid lines are the best fit of the data.

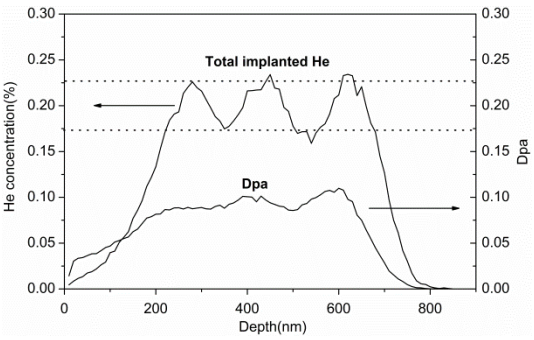


Fig.1. SRIM calculations for the He implantation, with the concentration 0.2 at.% and displacement damage 0.1 dpa.

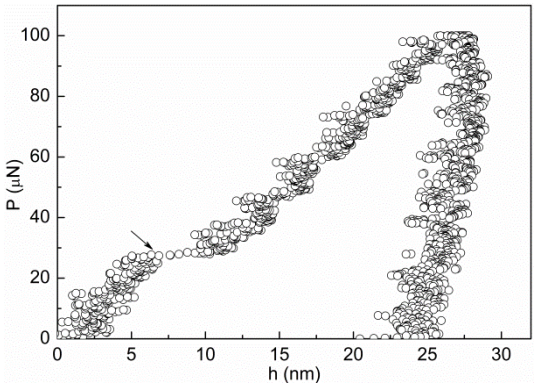


Fig. 2. A typical load-displacement (P-h) curve for nanoindentation. The arrow indicates the first displacement burst.

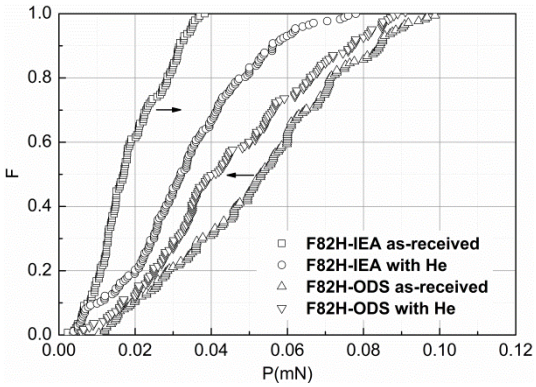


Fig. 3. The plot of the cumulative fraction, F, and applied loads, P, at the burst point.

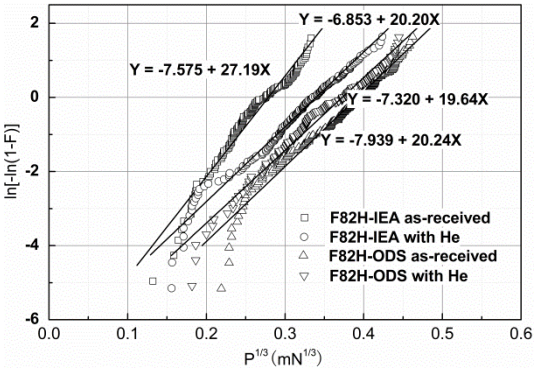


Fig. 4. Linear relation used to extract the activation volume. The solid lines are the best fit of the data.

Table 1.

Chemical compositions and heat treatment conditions of F82H-IEA and F82H-ODS steels (mass%).

| | C | Si | Cr | W | V | Ta | Ti | $Y_2O_3$ | Ex. O |
|---|---|---|---|---|---|---|---|---|---|
| F82H-IEA[a] | 0.090 | 0.11 | 7.71 | 1.95 | 0.16 | 0.02 | – | – | – |
| F82H-ODS[c] | 0.16 | 0.013 | 7.85 | 1.9 | 0.18 | 0.10 | 0.19 | 0.368 | 0.092 |

F82H-IEA: normalized at 1040C for 38min and tempered at 750C for 1h

F82H-ODS: normalized at 1050C for 1h and tempered at 750C for 1h.

Table 2.

Activation volume of the four samples.

| | $\Delta V(A^3)$ |
|---|---|
| F82H-IEA | 521 |
| F82H-IEA+He | 387 |
| F82H-ODS | 397 |
| F82H-ODS+He | 409 |